Electronic Supplementary Material (ESI) for Physical Chemistry Chemical Physics.


**Supplementary Information**

# Assembly and Relaxation Behaviors of Phosphatidylethanolamine Monolayers Investigated by Polarization and Frequency Resolved SFG-VS

*Feng Wei**[†], Wei Xiong, Wenhui Li, Wangting Lu, Heather C. Allen, Wanquan Zheng*

## 1. Experimental details of π-A isotherm and BAM detections

Three PE lipids: DMPE, $D_{54}$-DMPE and DPPE (Avanti lipids, purity> 99%) were analyzed in this study. The lipid solutions for spreading were prepared using the mixing solute of $CHCl_3$: Methanol = 4:1. For each isotherm experiments, about 35 ul lipid solution (1 mM) were spread on the surface of deionize water (Milli-Q Academic). The Langmuir isotherm of DMPE and DPPE monolayers were collected by KSV Teflon mini Trough with a compression speed of 5mm/min. The same Langmuir trough was also used in SFG-VS detection to control the SP of monolayer. For SFG spectra collection at stabilized SP value ( ± 0.3 mN/m), the compression speed of ± 3 mm/min was used. For the compression kinetics detection, the compression speed was 27 mm/min.

BAM images of the monolayers were collected simultaneously with π-A isotherms using a custom-built BAM. The laser source (Research Electro-Optics) emits 5 mW p-polarized light at 543 nm. The incident beam is first attenuated by a half-wave plate and then filtered by a Glan-Thompson polarizer before reaching the aqueous surface at the Brewster angle (~53°). The reflected beam is collected by an infinity-corrected Nikon 10° objective lens and is then focused by a tube lens. A back-illuminated electron multiplying CCD camera (Andor, model DV887-BV, 512 × 512 pixels) was used to record BAM images. The inclined position of the imaging optics

results in images focused along a central narrow stripe. Final images taken were cropped from a 800 μm × 800 μm size to show the most resolved regions, which was typically the center of the image where the beam was the most intense.

## 2. SFG spectra of ODT monolayers

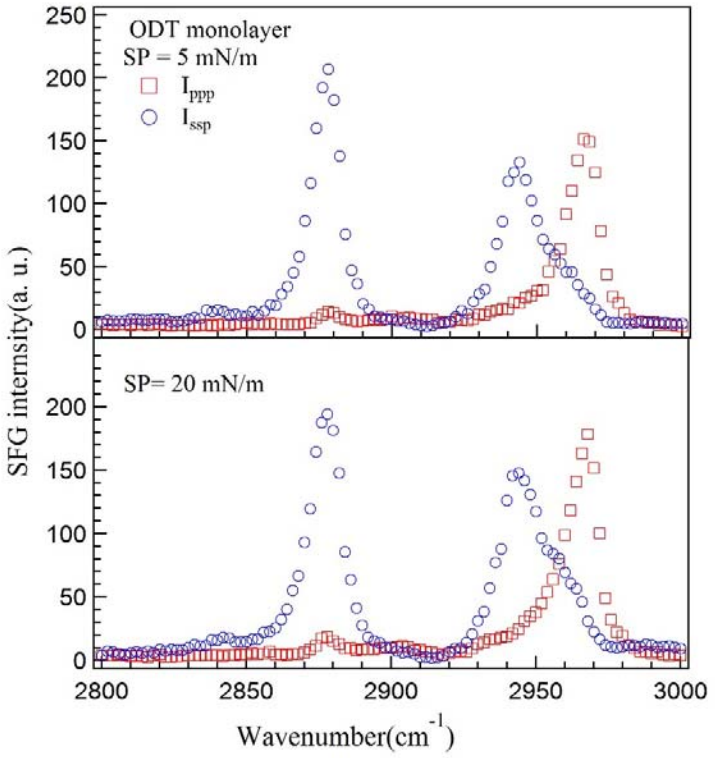


Figure S1. SFG spectra of ODT monolayer at SP = 5 mN/m and 20 mN/m in the wavenumber range of 2800-3000 $cm^{-1}$.

## 3. Fitting of SFG-VS Signals

As described in detail elsewhere, the intensity of the SFG light is proportional to the square of the sample's effective second-order nonlinear susceptibility( $\chi_{eff}^{(2)}$ ), and the intensity of the two input fields $I_1(\omega_{vis})$ and $I_2(\omega_{IR})$, see eq. (S1), which vanishes when a material has inversion symmetry.[1-7]

$$I(\omega_{SFG}) \propto \left|\chi_{eff}^{(2)}\right|^2 I_1(\omega_{vis}) I_2(\omega_{IR}) \qquad \text{(S1)}$$

where $\omega_{SFG} = \omega_{IR} + \omega_{vis}$. As the IR beam frequency is tuned over the vibrational resonance of surface/interface molecules, the effective surface nonlinear susceptibility $\chi_R^{(2)}$ can be enhanced. The frequency dependence of $\chi_{eff}^{(2)}$ is described by eq. (S2)

$$\chi_{eff}^{(2)}(\omega) = \chi_{NR}^{(2)} + \sum_{\upsilon} \frac{A_\upsilon}{\omega - \omega_\upsilon + i\Gamma_\upsilon} \qquad \text{(S2)}$$

where $A_\upsilon$, $\omega_\upsilon$, and $\Gamma_\upsilon$ are the strength, resonant frequency, and damping coefficient of the vibrational mode($\nu$), respectively. $A_\upsilon$ could be either positive or negative depending on the phase of the vibrational mode. The plot of SFG signal vs. the IR input frequency shows a polarized vibrational spectrum of the molecules at surface or interface. $A_\upsilon$, $\omega_\upsilon$, and $\Gamma_\upsilon$ can be extracted by fitting the spectrum. The fitting parameters of SFG spectra of DMPE monolayer at 3mN/m and 20 mN/m are listed in table S1 for demonstration.

Table S1 Fitting parameters of SFG spectra of DMPE monolayer at 3mN/m and 20 mN/m

| SP | | 3 mN/m | | 20 mN/m | |
|---|---|---|---|---|---|
| Polarization | | PPP | SSP | PPP | SSP |
| $A_0$ | | 0.65 ± 0.09 | 0.54 ± 0.09 | -0.39 ± 0.07 | -0.74 ± 0.29 |
| Peak 1 | $A$ | -32.07 ± 16.23 | 10.29 ± 7.66 | | |
| | $\omega_0$ | 2837.1 ± 2.4 | | | |
| | $\Gamma$ | 16.9 ± 5.8 | | | |
| Peak 2 | $A$ | -18.63 ± 4.87 | -33.24 ± 2.19 | 14.87±1.22 | 13.98 ± 1.47 |
| | $\omega_0$ | 2855.0 ± 0.4 | | 2848.5 ± 0.9 | |
| | $\Gamma$ | 7.6 ± 0.4 | | 8.4 ± 0.6 | |
| Peak 3 | $A$ | 9.79 ± 1.51 | -38.41 ± 1.84 | -18.92 ± 2.09 | 110.93 ± 2.23 |
| | $\omega_0$ | 2882.1 ± 0.2 | | 2880.8 ± 0.1 | |
| | $\Gamma$ | 4.9 ± 0.2 | | 6.2 ± 0.1 | |
| Peak 4 | $A$ | -2.69 ± 1.98 | -5.34 ± 2.45 | -24.22 ± 5.85 | 31.27 ± 6.70 |
| | $\omega_0$ | 2930.2 ± 0.8 | | 2901.6 ± 0.7 | |

| | | | | | |
|---|---|---|---|---|---|
| | $\Gamma$ | 4.7 ± 1.8 | | 10.2 ± 1.7 | |
| | $A$ | 2.44 ± 2.04 | -53.81 ± 3.58 | -25.10 ± 2.73 | 120.95 ± 3.79 |
| Peak 5 | $\omega_0$ | 2947.1 ± 0.4 | | 2943.4 ± 0.2 | |
| | $\Gamma$ | 7.8 ± 0.4 | | 9.0 ± 0.2 | |
| | $A$ | 5.50 ± 1.70 | -5.93 ± 2.33 | -18.36 ± 5.16 | 7.09 ± 2.89 |
| Peak 6 | $\omega_0$ | 2957.8 ± 0.3 | | 2957.2 ± 0.4 | |
| | $\Gamma$ | 3.7 ± 0.8 | | 5.6 ± 1.0 | |
| | $A$ | -37.50 ± 1.54 | 2.87 ± 1.31 | 74.23 ± 1.82 | -15.83 ± 1.91 |
| Peak 7 | $\omega_0$ | 2970.4 ± 0.2 | | 2970.1 ± 0.2 | |
| | $\Gamma$ | 4.4 ± 0.2 | | 5.1 ± 0.1 | |
| $C_0$ | | 4.67 ± 0.42 | 1.25 ± 0.99 | 4.89 ± 1.1 | -4.85 ± 1.21 |

## 4. Tilt angle analysis

The molecular orientation information can be obtained by relating SFG susceptibility tensor elements $\chi_{ijk}(i,j,k=x,y,z)$ to the SFG molecular hyperpolarizability tensor elements $\beta_{lmn}(l,m,n=a,b,c)$.[4-6] The components of $\chi_{eff}^{(2)}$ of ssp, and ppp polarization combinations are given in equations (S5)-(S6) in the lab coordinate system which is defined as the z-axis being along the surface normal and the x-axis being in the incident plane.[4-6]

$$\chi_{eff,ssp}^{(2)} = L_{yy}(\omega_{SF})L_{yy}(\omega_{Vis})L_{zz}(\omega_{IR})\sin\beta_{IR}\chi_{yyz}^{(2)} \qquad \text{(S3)}$$

$$\begin{aligned}\chi_{eff,ppp}^{(2)} = &-L_{xx}(\omega_{SF})L_{xx}(\omega_{Vis})L_{zz}(\omega_{IR})\cos\beta_{SF}\cos\beta_{Vis}\sin\beta_{IR}\chi_{xxz}^{(2)}\\ &-L_{xx}(\omega_{SF})L_{zz}(\omega_{Vis})L_{xx}(\omega_{IR})\cos\beta_{SF}\sin\beta_{Vis}\cos\beta_{IR}\chi_{xzx}^{(2)}\\ &+L_{zz}(\omega_{SF})L_{xx}(\omega_{Vis})L_{xx}(\omega_{IR})\sin\beta_{SF}\cos\beta_{Vis}\cos\beta_{IR}\chi_{zxx}^{(2)}\\ &+L_{zz}(\omega_{SF})L_{zz}(\omega_{Vis})L_{zz}(\omega_{IR})\sin\beta_{SF}\sin\beta_{Vis}\sin\beta_{IR}\chi_{zzz}^{(2)}\end{aligned} \qquad \text{(S4)}$$

where $\beta_{SF}$, $\beta_{Vis}$ and $\beta_{IR}$ are the angles between the surface normal and the sum frequency beam, the input visible beam, and the input IR beam, respectively. $L_{ii}$ (i = x, y or z) denotes the Fresnel coefficients. Under current experimental geometry, after considering the Fresnel coefficient constants, eqs.(S5-S6) are then given by

**$CH_3$ groups:**

$$\chi_{eff,ssp}^{(2)} = 0.249\chi_{yyz}^{(2)} \qquad \text{(S5)}$$

$$\chi^{(2)}_{eff,ppp} = \text{-}0.159\chi^{(2)}_{xxz} + 0.226\chi^{(2)}_{zzz} \quad \text{(S6)}$$

**$PO_2^-$ groups:**

$$\chi^{(2)}_{eff,ssp} = 0.244\chi^{(2)}_{yyz} \quad \text{(S7)}$$

$$\chi^{(2)}_{eff,ppp} = \text{-}0.156\chi^{(2)}_{xxz} + 0.225\chi^{(2)}_{zzz} \quad \text{(S8)}$$

### 3.1. $CH_3$ groups.

Here we treated $CH_3$ groups as $C_{3v}$ symmetry The SFG susceptibility tensor elements $\chi_{ijk}(i,j,k=x,y,z)$ of $C_{\infty v}$ symmetry have following relationships.[4-6]

$$\chi^{(2)}_{xxz,ss} = \chi^{(2)}_{yyz,ss} = \frac{1}{2}N_s\beta_{ccc}[(1+R)\langle\cos\theta\rangle - (1-R)\langle\cos^3\theta\rangle] \quad \text{(S9)}$$

$$\chi^{(2)}_{zzz,ss} = N_s\beta_{ccc}[R\langle\cos\theta\rangle + (1-R)\langle\cos^3\theta\rangle] \quad \text{(S10)}$$

$$R = \frac{1+r-(1-r)\cos^2\tau}{2(r+(1-r)\cos^2\tau)} \quad \text{(S11)}$$

$$\chi^{(2)}_{xxz,as} = \chi^{(2)}_{yyz,as} = -N_s R'\beta_{ccc}(\langle\cos\theta\rangle - \langle\cos^3\theta\rangle) \quad \text{(S11)}$$

$$\chi^{(2)}_{zzz,ss} = 2N_s R'\beta_{ccc}[\langle\cos\theta\rangle - \langle\cos^3\theta\rangle] \quad \text{(S12)}$$

$$R' = \frac{\beta_{aca}}{\beta_{ccc}} = \frac{-(1-r)\sin^2\tau\dfrac{G_{as}}{\omega_{as}}}{2(r+(1-r)\cos^2\tau)\dfrac{G_{ss}}{\omega_{ss}}} \quad \text{(S13)}$$

The parameter $R$ is estimated to be 3.338 when r = 0.03 and $\tau = 109.5°$, and the parameter $R'$ is estimated to be 2.80.[7] By substitution of eqs. (S9)-(S10) in eqs.(S7)-(S8), the deduced susceptibility ratio $\chi^{(2)}_{ssp,CH_3-ss} / \chi^{(2)}_{ssp,CH_3-as}$ can be plotted as a function of orientation angle (θ) (shown in Figure S2).

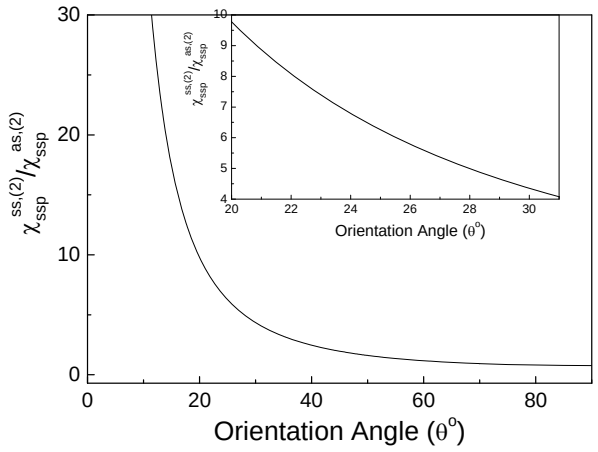


Figure S2 Deduced susceptibility ratio of $\chi^{(2)}_{ssp,\mathrm{CH_3}-ss}$ / $\chi^{(2)}_{ssp,\mathrm{CH_3}-as}$ is plotted as a function of orientation angle (θ) for the $CH_3$ groups which was treated as having $C_{3v}$ symmetry.

### 3.2. $PO_2^-$ groups.

The symmetry of $PO_2^-$ group can be treated as $C_{2v}$ symmetry. The peaks at ~ 1100 $cm^{-1}$ can be assigned to $A_1$ modes.[8-10] The susceptibility tensor elements of $A_1$ mode in $C_{2v}$ symmetry are described as following equations.[4-6]

$A_1$ mode:

$$\chi^{(2),A1}_{xxz} = \chi^{(2),A1}_{yyz} = \frac{1}{2}N_s\beta_{ccc}[\langle\cos^2\psi\rangle R_a + \langle\sin^2\psi\rangle R_b + 1]\langle\cos\theta\rangle + \frac{1}{2}N_s\beta_{ccc}[\langle\sin^2\psi\rangle R_a + \langle\cos^2\psi\rangle R_b - 1]\langle\cos^3\theta\rangle \quad \text{(S14)}$$

$$\chi^{(2),A1}_{zzz} = N_s\beta_{ccc}[\langle\sin^2\psi\rangle R_a + \langle\cos^2\psi\rangle R_b]\langle\cos\theta\rangle - N_s\beta_{ccc}[\langle\sin^2\psi\rangle R_a + \langle\cos^2\psi\rangle R_b - 1]\langle\cos^3\theta\rangle \quad \text{(S15)}$$

where $\psi$ is the twisting angle of $PO_2^-$ group. Using the bond polarizability derivative model, the polarization ratios of $R_a$ and $R_b$ of $O\cdots P\cdots O$ stretch in pyridine ring is determined by taking $r_{P\text{-}O}$ = 0.54(corresponding Raman depolarization ration is 0.33) and τ=120°.[11]

$$R_a = \frac{\beta_{aac}}{\beta_{ccc}} = \frac{1 + r - (1 - r)\cos\tau}{1 + r + (1 - r)\cos\tau} \quad \text{(S16)}$$

$$R_b = \frac{\beta_{bbc}}{\beta_{ccc}} = \frac{2r}{1+r+(1-r)\cos\tau} \qquad \text{(S17)}$$

According to eqs.(S16) and (S17), the deduced susceptibility ratio $\chi^{(2)}_{ppp,PO_2^-\text{-}ss} / \chi^{(2)}_{ssp,PO_2^-\text{-}ss}$ at $\psi = 0°$ can be plotted as a function of the tilt angle (shown in Figure S3).

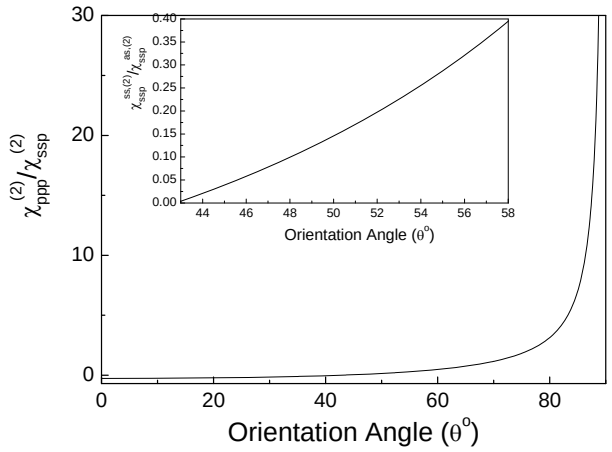


Figure S3 The deduced susceptibility ratio $\chi^{(2)}_{ppp,PO_2^-\text{-}ss} / \chi^{(2)}_{ssp,PO_2^-\text{-}ss}$ is plotted as a function of the tilt angles of $PO_2^-$ group treating $O \doteq P \doteq O$ bond as having $C_{2v}$ symmetry.

## 5. $R^{1105\text{cm}^{-1}}$ and $R^{2970\text{cm}^{-1}}$ of DMPE and DPPE monolayers

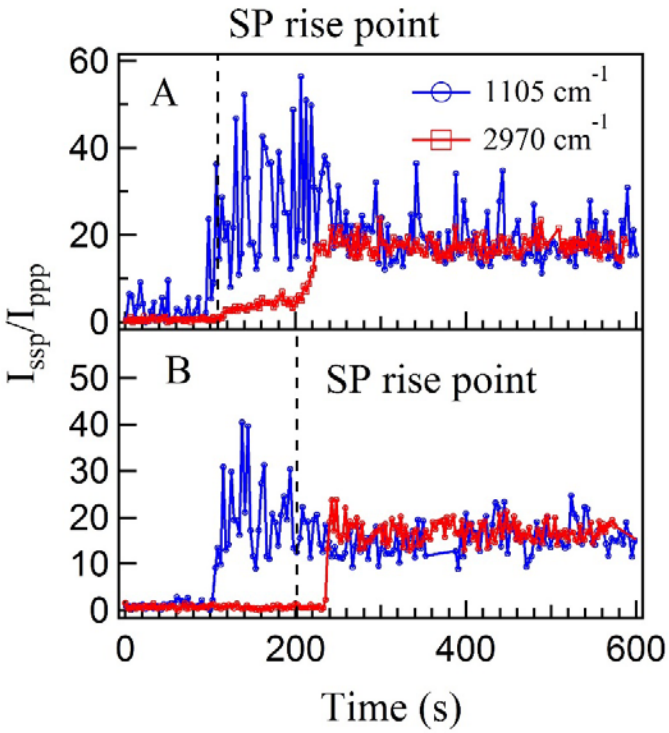


Figure S4. $R^{1105\text{cm}^{-1}}$ and $R^{2970\text{cm}^{-1}}$ of A). DMPE and B). DPPE monolayers during the compression

**References**

1. Antonov L.; Nedeltcheva, D. *Chem. Soc. Rev.,* **2000**, 29, 217–227.

2. Crisponi, G. *React. Funct.l Polym.,* **1997**, 34, 121-126.

3. Ghasemi, J.; Niazi, A.; Kubista M.; Elbergali, A. *Analyt. Chim. Acta,* **2002**, 455, 335–342.

4. Shen, Y. R. The Principles of Nonlinear Optics; John Wiley& Sons: New York, **1984**.

5. Lambert, A. G.; Davies P. B.; Neivandt, D. J *Appl. Spectrosc. Rev.,* **2005**, 40, 103–145.

6. Wang, H. F.; Gan, W.; Lu, R.; Rao, Y.; Wu, B. H. *Int. Rev. Phys. Chem.* **2005**, 24, 191–256.

7. Biswas N.; Umapathy, S.; *J. Chem. Phys.,* **1997**, 107, 7849-7858.

8. Castellucci, E.; Sbrana G.; Verderame, F. D. *J. Chem. Phys.,* **1969**, 51, 3762-3770.

9. Moskovits, M.; DiLella D. P.; Maynard, K. J. *Langmuir,* **1988**, 4, 61-76.

10. Golab, J. T.; Sprague, J. R.; Carron, K. T.; Schatz G. C.; Van Duyne, R. P. *J. Chem. Phys.,* **1988**, 88, 7942-7951.
11. Chen, C. Y.; Liu, W. T.; Pagliusi, P.; Shen, Y. R. *Macromolecules,* **2009**, 42, 2122-2126.